NFRA

USER DOCUMENTATION

PART IV

CALIBRATION AND
REDUCTION OF WSRT DATA

July 16, 1993

Version: 1.0.0

WEST

EAST

0 1 2 3 4 5 6 7 8 9 A B 300m

C D
160m
72 m

a 72m

9x144m=1296m

1368+a 1224m

2664+a
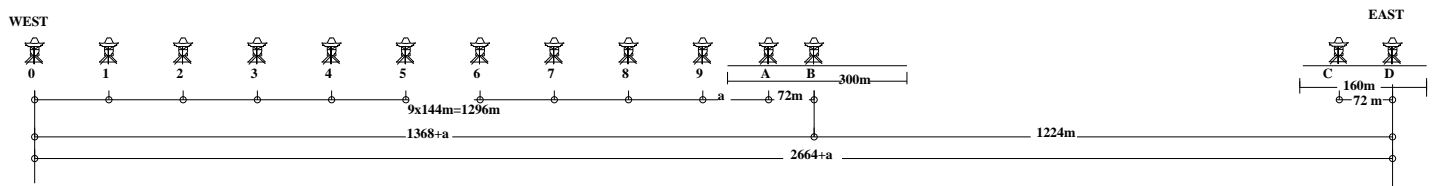
WSRT

CONTENTS OF PART IV

This is part IV of the WSRT User Documentation.
The WSRT User Documentation consists of 7 Parts; we may refer to other parts of the User Documentation. To get more information about how to obtain a copy and/or updates of parts of the User Documentation please send an e-mail request to `wsrt@nfra.nl`
The roman number in the pagenumber indicates the part.

WSRT

USER DOCUMENTATION

CALIBRATION OF WSRT DATA

Ed. O.M. Kolkman, texts supplied by A.R. Foley, T.A.Th. Spoelstra and H.W. van Someren-Gréve

The (u, v) data require a number of corrections before we can make a radio map, which can be used for scientific interpretation. A number of corrections are applied on–line in Westerbork. The first section of this chapter will describe those. The second section of this chapter deals with the post observation corrections. The corrections are described in more detail in a technical report by Brouw (1974, further referred to as ITR78)

1.1 ON-LINE CORRECTIONS

The basic philosophy is that all a-priori known errors, and all those errors which, if not applied, will damage the observations, must be corrected on-line as much as possible. Many of the on-line correction factors will be improved off line after the observation, also added then are those corrections which are not, or better known than at the time of the observation.

1.1.1 THE ON-LINE CORRECTIONS

Below we will describe which corrections are performed on-line.

1. **Pointing.**

   In order to keep all the telescopes at the requested position during the observation, a set of pointing corrections is applied. There are two different correction algorithms used in combination . The correction also implies a correction for the pointing error due to refraction.

   (a) A model

      For each telescope the pointing error in hour angle, h, and declination, δ, is described by a small set of model parameters.

      The model describes the error in terms of offset, $\sin(\delta)$, $\cos(\delta)$, $\cos(h)$, $\sin(\delta)\cos(h)$, $\cos(\delta)\cos(h)$, $\sin(h)$, $\sin(\delta)\sin(h)$, and $\cos(\delta)\sin(h)$ coefficients.

   (b) A table The model turned out not to be able to describe the real pointing behavior of the telescopes sufficiently accurate. After September 1987 an additional pointing correction as a function of hour angle and declination was introduced.

      This extra correction is derived every 10 sec from a linear interpolation of the nearest points in a table which contains for every telescope the pointing errors in hour angle and declination for every 5 degrees in hour angle and declination, over the full part of the sky that can be reached by Westerbork telescopes.

2. **Precession, nutation, and aberration.**

The epoch coordinates, supplied by the astronomer are converted to apparent coordinates for a moment, t, near the middle of his observation.

Also calculated for that moment are the first derivative in time of the position vector. In this derivative vector all effects related to precession and nutation are taken into account, except the diurnal aberration.

For every 10 seconds the actual apparent position vector is calculated, using the position vector at time t, its first derivative, and the diurnal aberration.

3. **Phase corrections.**

There are many effects that cause errors in the phase of the data. The phase error of each effect is calculated per receiver (or IF channel), for each 10 second interval, summed per effect, and added to the natural fringe phase, which is send to the primary fringe demodulator device.

These effects are :

(a) A constant phase error per IF.

(b) The effects of a position error of each telescope with respect to an ideal East-West line at the given geographic coordinates of the Westerbork array.

(c) The effect of an extrapolated clock and baseline pole error.

(d) The effects caused by an error in the orientation of the polar axis of each telescope with respect to the equatorial North Pole.

(e) The effects caused by refraction of the signal propagating through a curved atmosphere.

(f) Sign reversal correction depending on the down mixing convention of the observed frequency to IF frequency.

4. **Amplitude corrections.**

These corrections include all effects that influence the amplitudes of the observed signals, and converts the amplitude to units of 5 mJy (Westerbork units).

These effects are :

(a) The quantization (or Van Vleck) correction, which transforms the normalized measured correlation coefficients into analog correlation coefficients, depending on the correlator bit mode used (2x2, 2x3, 2x4, 4x3, 4x4, or 3x3).

(b) Derive the system temperature from the measured Total Power values with a noise source of known temperature, and without a noise source, per IF unit.

Use the system temperature for the correction of the normalized analog correlation coefficients to Westerbork units. This correction occurs per IF unit.

(c) A correction for extinction.

5. **Delay corrections.**

Delay errors decorrelate the signal, and have to be corrected before a continuum point is made from the frequency points. The geometrical delay is calculated and taken into account every 10 sec.

A fixed table with delay offsets is used once per observation, there is however a difference depending on the correlator.

(a) DLB/DXB

The delay offset is set per telescope, i.s.o. per IF. Unfortunately there are some delay offset differences between the 2 IF channels of the same telescope. These differences cause a phase slope over the pass band. This phase slope will be removed in the on-line system.

(b) DCB

The delay offset table has an entry for each IF and each band.

6. **DC offsets correction.**

   A fast phase switch device, which switches the phase with 180 degrees with 6.4 Hz in the primary fringe demodulation device (modulation), and corrects for the 180 degree phase insertion (demodulation) after correlation, corrects for DC offsets in the system. This is especially important for the DCB.

7. **Frequency correction.**

   For line observations with the DLB/DXB the proper apparent frequency for a specified rest frequency of a spectral line is calculated and send to a frequency synthesizer. During the observation this frequency is changed, due to the differential motion of the WSRT with respect to the velocity reference system.

8. **Fourier transform effects.**

   These effects only concern the DLB/DXB, where a Fourier transform from time to frequency is done.

   The truncation of the correlation function causes a ripple in the spectrum, which cannot be calibrated because it is a function of the observed phase.

   It is possible to make the ripple independent of the phase, and hence enable calibration, by implementing a 90 degree phase switch in the primary fringe demodulation device in every odd 10 sec, and correcting for this in the software.

   However this will only help if the integration time is an even number of 10 sec periods, and the correlator configuration only contains standard interferometers (i.e. interferometers between fixed and movable telescopes).

9. **Uncorrectable errors.**

   With a complicated instrument like the WSRT it is unavoidable that we have from time to time some malfunctioning of its components, which will lead to completely wrong data. If the on-line system notices this, the data will be deleted. Deletion of the data will consist in the substitution of integer value -32768 for both cosine and sine.

   This will happen in the following cases :

   (a) All data for a telescope which is out of operation, or is not following the requested position anymore.

   (b) If one or more of the channels of the correlator is bad, the correlation function (or interferometer-polarization channel data) to which these channels belong are deleted.

   (c) Extreme cases, where the shadowing of the telescopes becomes too much, or the telescopes are looking near the horizon or to negative elevation angle.

   (d) In general all correlator data as read from the correlator are directly converted to a floating point number, and all corrections are applied in floating point form. However the output is in fixed point form (16 bit), so if the conversion from floating point to fixed point lead to values outside the fixed point range, this data is deleted. Normally with the correct calibration parameters this will not happen. But it can occur for instance when the data are affected by man made interference (EMI).

1.1.2   THE DETERMINATION OF CORRECTION PARAMETERS.

The correction parameters which are applied to the observed data have to be determined prior to the observation. Determination of these parameters require a number of special calibration observations, which the astronomer usually never sees, except for a short calibration observation directly before and after his observation. We will discuss these observations.

1. **Pointing.**

   Determination of the pointing model and table require a large number of observations, which can best be done at an observing wavelength of 6 cm.

   In each of these observations a group of telescopes observes at 4 positions around, and one on a calibrator source, while the other group of telescopes remain on the calibrator, after that the pattern is reversed.

   A typical duration of such an observation is 18 minutes.

   A single observation like this is sufficient to determine a pointing offset for RA and dec.

If one wants to determine a much better check of the pointing behavior, many pointing observations spread evenly over the whole sky are necessary, which takes at least 24 hours.

The pointing behavior repeats itself at least within 0.6 arcminutes, and on the average within 0.2 arcminutes.

A number of special programs have been developed to derive pointing parameters from these observations.

2. **Noise source temperatures.**

   The temperature of the noise sources can be calibrated with Total Power observations on the strongest sources in the sky, like Cas A, Cyg A, and Tau A.

3. **Telescope positions.** Calibrating the telescope positions require a large number of observations on calibrators with well known positions. Typically such a set of observations which must evenly cover the whole sky will take about 24 hours with observations of a duration of about 30 minutes.

   The software for interpretation of these data exist in Dwingeloo.

4. **Baseline pole and clock information.**

   From information about polar motion and UT1-UTC from the International Earth Rotation Service (IERS) received on a weekly basis, the corrections for baseline pole and clock are determined from extrapolation. The extrapolation is at most over 2 weeks. The extrapolated values show errors of typical 0.005 arcsec in the baseline pole, and 3 milliseconds in time.

   These corrections are checked off-line in Dwingeloo.

5. **Delay offsets.**

   Every calibrator observation with the DLB/DXB in which all frequency points are kept can serve for a delay offset determination. A special program interpret the phase slopes over the pass bands, and derives the delay offsets per IF. For measuring the delay offsets for the DCB we have to perform a special observation on a calibrator in which the delay is changed per integration time. The amplitude plotted data as a function of time shows the decorrelation function. A special program interprets these observation into delay offsets per band and per IF.

6. **ionosphere**

   No corrections for ionospheric effects are determined and applied in Westerbork, since it is not possible to obtain ionospheric information in real time. The Westerbork off-line reduction takes care of this effect,

1.1.3   CHECK OF THE ON-LINE CORRECTIONS

After the observation is done, there are a number of programs that check the quality of the observation, and the related calibration observations.

1. Make a map.

   A spatial Fourier transform program makes a small map of the central part of the field of typically 180 x 180 points, without any cleaning, subtraction or further corrections.

2. Inspect the Total Power.

   It is possible to plot the receiver gain and system temperature (or Total Power values) for each IF as a function of hour angle. This will show the behavior of the front end during the observation.

3. Inspect the logging files of the on-line system.

   The on-line system checks many system parameters during the observation, and logs all abnormal results.

   The most important of these are the telescope positioning errors, and the correlator channel errors of the DLB/DXB. Software is available to display this information tabularly or graphically.

   There is also a display program that plots a requested set of correlation functions directly after they have been read out from the correlator by the on-line system.

4. Inspect phase and amplitude.

   This is useful only for the used calibration observations.

   Decomposing the amplitude and phase information from interferometer values into IF values shows the continuity of the system, and offers the possibility to determine improved zero values. Also amplitude and phase, as well as cosine and sine values can be displayed against hour angle in various ways.

1.2   POST OBSERVATIONAL CORRECTIONS OF WSRT DATA AT NFRA

Part of NFRA service is the possibility to have your WSRT data being corrected and calibrated, this will be done at request. The data can be calibrated, reduced and manipulated with several software packages: e.g. AIPS, NewStar, standard reduction package. The recommended off-line processing (*i.e.* applications of additional correction and calibration) is shown in figure 1.1.

Starting on the top left-hand corner of the diagram we see our input, the WSRT synthesis observations. These are raw $u - v$ data which have been corrected on-line. If the scientist needs high dynamic range measurements (that is a dynamic range > 1000) he needs to self-calibrate the data. This can be done with AIPS or the NewStar package (see also the NewStar cookbook, part **??**).

If you want to calibrate mosaic data or just want to do the calibration yourself, you should request your data from the head of the reduction group, together with calibration information.

If dynamic range better than 1000:1 is not needed and one does not want to mosaic or reduce the data oneself then one can ask for standard reduction. The reduction is performed using the standard reduction software. Any necessary corrections are applied.

These standard corrections (ITR78) are described below. Requests for standard reduction should be sent to A.R. Foley (after you have been informed that your data is available).

Dipole corrections

   In practice, there is always crosstalk between dipoles of a telescope. In Westerbork we try to minimize this but if you need to measure the polarization of a radiation from a source accurately (better than 0.5%) the crosstalk needs to be accurately measured and removed. This is done by observing sources of known polarization at different dipole settings ($++$ and $+\times$). These crosstalk terms are then calculated and removed off-line.

Baseline corrections

   In order to fill the UV plane we need to move the telescopes on the rail tracks. When positioning them, errors can be made in the precise placing of the telescopes ($\approx$3mm) which is not known when the fringe stopping is done. Hence a phase error with a sinusoidal pattern is introduced. This is clearly most important for short wavelengths (6, 21 cm) and less important for long (49, 92 cm). Similarly errors in the assumed UT1-UTC (clock errors) and errors in the assumed position of the baseline pole can lead to such patterns. These are determined using a "baseline package" of 24 hours of short observations of calibration sources with known accurate positions to calculate the telescope position errors (in 3-D). This is normally done immediately after a baseline shift at 6 or 21cm. Ideally one should take into account the (tiny) shift in uv coordinate also.

Atmospheric corrections:

   Radio interferometric observations are affected by tropospheric and ionospheric extinction and/or refraction. At radio frequencies below about 6 GHz tropospheric refraction is basically independent of frequency, while ionospheric refraction varies in inverse proportion to the observing frequency squared. The errors due to the tropospheric refraction becomes negligible small in comparison with that due to ionospheric refraction at frequencies below 1 GHz. (Spoelstra 1992).

   Ionosphere

      The effects of ionospheric refraction are visible in two ways:

      1. as phase errors, which are to first approximation (as long as the ionosphere is 'coherent' over the interferometer baseline) linearly proportional to the baseline length in meters;

START
WSRT synthesis observations

dynamic range > 1000 possible or needed ? — yes → Self calibrate using NEWSTAR → STOP

no

mosaic mode ? — yes → NEWSTAR with external calibrators → STOP

no

Do I want to calibrate the data myself ? — yes

no   [Standard reduction begins below]

Acurate (<0.5%) polarization needed ? — yes → Request dipole offset checks

no

Wavelength <30 cm ? — yes → Request baseline corrections

no

Request ionospheric refraction correction

Do I need polarization ? — yes → Request ionospheric Faraday rotation corrections

no

is shadowing relevant ? — yes → correct for shadowing ? — no → Delete shadowed baseline ? — no

no   yes   yes

Request shadowing correction   Request shadowing delete

A

A

Standard gain/phase calibration — yes → Request standard gain/phase calibration

no

[choise of output format]

map in AIPS — yes → Request UV FITS in Stokes parameters

no

map with LINEMAP in Leiden — yes → Request EBCDIC WSRT format

no

map with NEWSTAR or R-series — yes → Request ASCII WSRT format

no

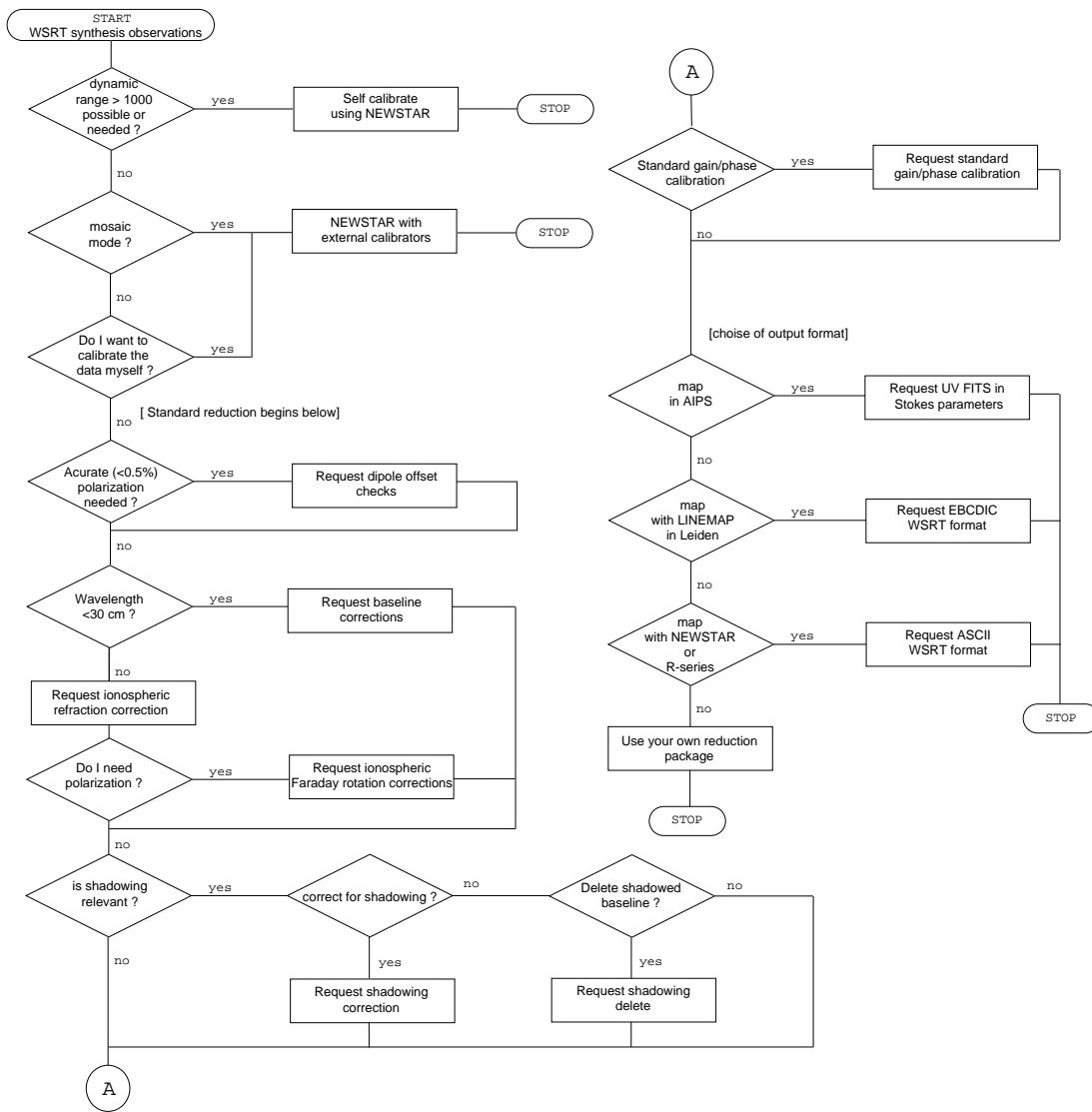Use your own reduction package

STOP

STOP

Figure 1.1: Flow chart with decisions that need to be made during the off-line data (standard) correction and calibration of WSRT observations

2. as Faraday rotation on polarized signals traveling through the ionosphere which is a magnetoionic medium.

The fundamental phenomenon is a delay error. In interferometry it translates into fringe rate or phase errors. Ionospheric refraction is a significant effect for connected element interferometry at frequencies up to about 2GHz. (Spoelstra (1993), Spoelstra (1983) investigated the influence of ionospheric refraction using the WSRT.)

From the above we see that for wavelengths longer than 30 cm a correction needs to be made for the ionospheric refraction.

The ionospheric corrections are made in Dwingeloo on the basis of measurements of the ionospheric electron content by civil and military ionospheric observatories. The measurements are usually taken at hourly intervals. The corrections are satisfactory except for times around sunrise when the atmosphere is heated and the structure of the ionosphere changes rapidly.

Troposphere

The effects of the troposphere are extinction and refraction.

To calculate the effect of extinction two effects need to be considered; the observed intensity will decrease as a result of absorption and scattering of molecules and the observed antenna temperature will increase due to the air radiation. The effects are both a function of airmass and thus the zenith distance of the observation (ITR 78).

The error due to tropospheric refraction is a phase error (parameterized by e.g. Brouw 1971, Spoelstra 1992 or ITR78) which is also function of the zenith distance of the observation.

The first-order tropospheric extinction and refraction corrections are applied on-line at Westerbork. But because the dominant contribution to the tropospheric refraction error usually stems from the gradient in the water vapor content (Resch 1984) (which depends on the weather) these first order corrections may be incorrect by an amount of the order of several tenths of percents. Because of uncertainties in the tropospheric parameters monitored during the observation (*i.e.* humidity) an additional correction (to the first order on-line correction) is usually not made.

The first order correction for extinction also be off by a percentage on the order of percents. Note that additional corrections for extinction can be made within the NewStar package.[1]

Ionospheric and tropospheric gain and phase errors at time scales of the order of one hour can be reduced when calibration is done using redundant baseline solutions and/or self-cal, also see part **??**.

More information about the effect of the atmosphere, *i.e.* refraction in the ionosphere and extinction in the troposphere, can be found in e.g. chapter 13 'Propagation Effects' in the book by Thompson *et al.*(1986), chapter 5 'Calibration and Editing' by Fomalont and Perley in the book by Perley *et al.* (1989) and in articles by Spoelstra (1983, 1984 and 1992) which are based on measurements with the WSRT.

Shadowing corrections:

Because we use some baselines which are only slightly longer than the telescope diameter, for some ranges of hour angle and declination (particularly near $\delta = 0^\circ$ and $h = \pm 90^\circ$) one telescope is shadowing its neighbor as seen from the source. We can apply a shadowing correction which allows for the loss of gain and shift in uv coordinate which is useful for a point source at the field center, but is not applicable in the general case. The observers with shadowing occurring in their data should be extremely cautious of using shadowed data, especially for extended fields (the correction should change across the field, but doesn't).

Standard Gain/Phase:

The Standard gain and phase corrections are calculated on the basis of a group of calibration sources (usually 2 to 8) observed in the same mode as the main source, and immediately around it. The calibration is done per frequency channel per interferometer, and its interferometer basis spoils the

---

[1] Additional extinction corrections be made, — but are not made in practice, because self-cal can handle these problems — by fitting the appropriate functions (e.g. ITR 78) to the system temperatures which are monitored during the observation and are available on request at NFRA.

telescope dependence of corrections used in self-calibration schemes (as in AIPS or NEWSTAR). Typically the maps made will reach dynamic ranges of 1000:1 per polarization. If that is not good enough do not ask for standard reduction!. The spectral dynamic range is usually much better, often a few thousand.

EMI

Observations suffering from man-made interference (EMI) can be corrected automatically for impulsive interference. Affected data points are marked as if deleted, *i.e.* the cosine and sine values are put equal to -32768 (as 16 bit numbers)

After the data have been corrected (we are at the top right-hand corner of figure 1.1) we are ready to make a map. The observer needs to choose the output format for his u, v-data.

If you want to do your map making in AIPS request output in UV FITS format with the data written as Stokes parameters. If you want to make a map using LINEMAP in Leiden request EBCDIC format. One can also make maps using NewStar or the R-series software developed at NFRA/ASTRON, one needs to request the data in ASCII WSRT format then. If you do not want to use any of the above packages then you want to use your own data reduction package you should request the data in one of the above formats.

1.3 REFERENCES

Brouw, W.N. (1974): *NFRA internal tech. report*, **78** (available at NFRA).

Perley, R.A., Schwab, F. and Bridle, A.H. (Editors) (1989): *"Synthesis Imaging in Radio Astronomy"*. Astronomical Society of the Pacific.. ISBN:0-937707-23-6. (see also review in part II Chapter 9.1, Book 2).

Resch, G.M. (1984): 'Water vapour radiometry in geodetic applications', in *"Geodetic refraction, effects of electromagnetic wave propagation through the atmosphere"*, ed. F.K. Brunner, Springer Verlag, Berlin, pp.53.

Spoelstra, T.A.Th. (1983): *Astron.& Astrophys.* , **120**, pp. 313-321.

Spoelstra, T.A.Th. (1984): Radio Science, **19-no3.**, pp. 779-788.

Spoelstra, T.A.Th. (1992): 'Ionosphere and Troposphere seen through a Radio Interferometer' in *"Remote Sensing of the Propagation Environment"*, AGARD Conference Proceedings 502, Advisory Group for Aerospace Research & Development, Neuilly sur Seine, France.

Thompson, A.R., Moran, J.M. and Swenson Jr., G.W. (1986): *"Interferometry and Synthesis in Radio Astronomy"*. John Wiley & Sons, New York.. ISBN 0-471-80614-5. (see also review in part II Chapter 9.1, book 3).

WSRT

USER DOCUMENTATION

PART IV

CHAPTER 2

TIPS, HINTS AND FREQUENTLY ASKED QUESTIONS

This chapter contains tips hints etc for the different stages of map making.

2.1 REDUCING 21 CM LINE DATA

Based on a gipsy dc0 document REDLINE *by R.Sancisi, updated by Marc Verheijen and Olaf Kolkman*

2.1.1 INTRODUCTION

This chapter contains a tentative guideline for an interactive processing of HI line data (principally extragalactic) using the GIPSY package[1]. The reduction process is given in various steps. With each step the GIPSY command with which a task can be performed is indicated.

2.1.2 REDUCTION OF LINE DATA

TRANSFER MAPS FROM FITS FORMAT INTO A GIPSY CUBE

1. Load each map into one subset all subsets make up the cube.   — RFITS
2. Make a list of disk contents   — DISK
3. Measure beamwidths in antenna pattern (AP)   — ANTPAT
4. Inspect the headers of MAP and AP cubes   — HEADER

FIRST ASSESSMENT OF DATA QUALITY

1. Visual inspection of antenna pattern , of broadband channel 0 (if you have it) and of channel maps. Record maps as a movie in GIDS   — VIEW RECORD=Y
2. Estimate r.m.s.noise in a signal free area   — STAT

   Make profiles or XV-maps across a continuum point source in the field. Look for variations of intensity or position with velocity.   — VIEW, QPLOT, SLICE

---

[1]GIPSY: The Groningen Image Processing SYstem is developed at the Kapteyn Institute and available on the anonymous ftp-node kapteyn.astro.rug.nl(129.125.6.204)

FORM AND SUBTRACT CONTINUUM MAP

1. Estimate velocity extend of line emission by:

   (a) visual inspection of a sequence of channel maps (e.g.use GIDS movie at various speeds,or make mosaic)   — VIEW REC=Y, CPLOT

   (b) make a position-velocity (XV) map across the source of line emission (e.g. along major axis and through the center of a galaxy)   — SLICE

2. (a) Form an average of the line-free channels on both low and high velocity sides separately and make difference map to look for systematic differences.   — MEAN, SUB

   (b) If no systematic difference is found, form a mean continuum map from all the line-free channels.
                                                                                      — MEAN

   (c) Remove the continuum by subtracting the mean continuum map from all channel maps including those used to form the continuum. Do not overwrite the original data set.   — SUB,CONREM

   (d) If the continuum is frequency dependent, use CONREM to form (and subtract) the continuum as a function of frequency.   — CONREM

3. If not enough line-free channels are available ,use BLOT to cut out the line signal. Form and subtract the continuum using CONREM on the blotted data cube.   — BLOT, CONREM

4. Estimate r.m.s.noise in continuum map.   — STAT

5. Inspect all new continuum free maps and verify optimal choice of continuum channels. Check that no emission is present in channels already used for continuum.   — VIEW REC=Y

6. Estimate r.m.s.noise in the line channels. Compare the noise before and after the subtraction of the continuum.   — STAT

7. Make an average of all the line channels with no cutoff, and look for any systematic effects and errors(rings,DC-offsets etc)   — MEAN

STUDY OF HI SOURCE

1. Visual inspection of continuum free channel maps in velocity sequence (zoomed if necessary)
   — VIEW RECORD=Y

2. Use CLEAN to restore base level of maps and to get rid of disturbing side-lobes and/or grating rings.
   — CLEAN

3. Consider signal/noise ratio.Velocity and /or spatial smoothing may be necessary to improve signal/noise ratio of extended emission.   — SMOOTH,VELSMO

4. Global profile.

   (a) Integrate each channel map over a rectangular region containing HI emission and divide by the sum over the beam values in the same area centered on the antenna pattern. The size of the area may seriously affect the result.In cases of poor S/N ratio this integration can better be done after smoothing. Flux densities are corrected for primary beam attenuation.   — FLUX

   (b) As an alternative procedure decompose the HI source into CLEAN components and add the residual to the flux in the components. Apply primary beam correction.   — CLEAN

5. Total HI map and velocity field.

   (a) Quick sum of all the line channels (with or without cutoff;as cutoff use 1.5-3×rms) to obtain integrated HI map.   — SUM

   (b) Use MOMENTS or GAUFIT to obtain maps of integrated HI, velocity field and velocity dispersion.
       — MOMENTS, GAUFIT

   (c) Blotch the area of HI emission on displayed channel maps (points outside area are set to zero).
                                                                                      — BLOT

(d) or use smoothed data to define region of emission in unsmoothed maps. Then straight summation for HI,weighted sum for velocity field.   — CONDIT(& BLOT), MOMENTS

$$N_H(\text{atomscm}^{-2}) = 1.823 \times 10^{18} \times SUM\,T_b(\text{K}) \times DV(\text{km/s}) \qquad (2.1)$$

(DV is usually channel separation)

6. Total HI mass.

   (a) From global profile (preferable in general).

   (b) From integration of the total HI map over area of HI source (area in AP is usually too large)
       — FLUX

$$\frac{M(H)}{M_\odot} = 2.36 \cdot 10^5 D^2(Mpc) \times SUM\,S(Jy) \times DV(km/s) \qquad (2.2)$$

7. Conversion factor S(mJy)/Tb(K):
   Equivalent $T_b(K)$ for 1.0 mJy/synthesized beam area
   is :

$$\frac{687 \cdot (1420.4/\nu_{obs})^2}{(SUM\,AP \cdot DL(\text{arcsec}) \cdot DM(\text{arcsec}))}$$

   (DL, DM: gridspacing (arcsecs); 1WU = 5 mJY/BEAM; ν_{obs} is the observing frequency)

TIPS

1. Try SMOOTH and CLEAN also on the Antenna Pattern as a check.

2. Leave Primary Beam corrections on HI maps (channel or total HI) always as the last operation after , for instance, smoothing , cleaning , etc.

2.2 FREQUENTLY ASKED QUESTIONS

This section needs to be expanded. Please send your suggestions or questions, with or without answers to `wsrt@nfra.nl`.

Question *What is the noise in a total HI map ?*

Answer *by Marc Verheijen*

We will show how the noise in a total HI map can be calculated. A total HI map is usually constructed from a 3 dimensional datacube containing a number of so called channelmaps. Each channelmap shows an HI image of the galaxy at a certain velocity. A total HI map is made by adding those channelmaps which contain the HI signal. Before adding the channelmaps the signal in each channelmap must be isolated. When the signal is not isolated one merely adds noise to the total HI map because the location of the signal in a channelmap varies with velocity due to the galactic rotation. The signals can be isolated interactively using the BLOT program or in a more objective way using a certain contour level in the smoothed maps as a mask. As a consequence of adding channelmaps with isolated regions the noise in the total HI map is not constant but varies from pixel to pixel. The noise at a certain pixel in the total HI map depends on the number N of non-blank pixels at the same position in the individual channelmaps that were added.

In case the datacube was obtained with an uniform taper during the observation, the noise σ^u in two channelmaps will be independent. The noise equivalent bandwidth B^u in a uniform tapered spectrum is equal to the channel separation b. When adding N uniform tapered channelmaps at a certain pixel the noise σ_N^u at the same pixel position in the total HI map will be increased by a factor $\sqrt{N}$:

$$\sigma_N^u = \sqrt{N}\ \sigma^u$$

Usually, the observations are made using a Hanning taper in which case the noise in two adjacent channelmaps is no longer independent. A Hanning taper effectively smooths the data in velocity by convolving the velocity profile at each pixel. If U_i is the pixel value in the ith uniform tapered channelmap, the value H_i in the ith Hanning tapered channelmap is given by

$$H_i = \tfrac{1}{4}U_{i-1} + \tfrac{1}{2}U_i + \tfrac{1}{4}U_{i+1}$$

Since the σ_i^u's are independent and all equal to σ^u, the noise σ_i^h in the ith Hanning tapered channelmap can be calculated according to

$$
\begin{aligned}
\sigma_i^h &= \left[(\tfrac{1}{4}\sigma_{i-1}^u)^2 + (\tfrac{1}{2}\sigma_i^u)^2 + (\tfrac{1}{4}\sigma_{i+1}^u)^2\right]^{\frac{1}{2}} \\
&= \left[\tfrac{1}{16} + \tfrac{1}{4} + \tfrac{1}{16}\right]^{\frac{1}{2}} \sigma^u \\
&= \tfrac{\sqrt{6}}{4}\, \sigma^u = 0.61\, \sigma^u
\end{aligned}
$$

In this case the noise equivalent bandwidth B^h for a Hanning tapered spectrum is given by

$$B^h = \left(\tfrac{16}{6}\right) B^u = 2.67\, B^u$$

As a consequence, the noise in two Hanning tapered channelmaps may be correlated depending on their separation. Two channelmaps separated by one channelmap are correlated because both contain a quarter of the flux from the channelmap between them. Only every third channelmap is independent. This will be shown in the following three cases in which two Hanning taperd channelmaps at different separations will be added.

– Adding two adjacent Hanning tapered channelmaps i and (i+1) gives a signal $H_{(i)+(i+1)}$ of

$$
\begin{aligned}
H_{(i)+(i+1)} &= H_i + H_{i+1} \\
&= \left(\tfrac{1}{4}U_{i-1} + \tfrac{1}{2}U_i + \tfrac{1}{4}U_{i+1}\right) + \left(\tfrac{1}{4}U_i + \tfrac{1}{2}U_{i+1} + \tfrac{1}{4}U_{i+2}\right) \\
&= \tfrac{1}{4}U_{i-1} + \tfrac{3}{4}U_i + \tfrac{3}{4}U_{i+1} + \tfrac{1}{4}U_{i+2}
\end{aligned}
$$

And the noise $\sigma_{(i)+(i+1)}^h$ in that map will be

$$
\begin{aligned}
\sigma_{(i)+(i+1)}^h &= \left[(\tfrac{1}{4}\sigma_{i-1}^u)^2 + (\tfrac{3}{4}\sigma_i^u)^2 + (\tfrac{3}{4}\sigma_{i+1}^u)^2 + (\tfrac{1}{4}\sigma_{i+2}^u)^2\right]^{\frac{1}{2}} \\
&= \tfrac{\sqrt{20}}{4}\, \sigma^u = \tfrac{\sqrt{20}}{4}\tfrac{4}{\sqrt{6}}\, \sigma^h \\
&= \sqrt{3\tfrac{1}{3}}\, \sigma^h = 1.83\, \sigma^h
\end{aligned}
$$

– Adding the Hanning tapered channels i and (i+2) gives

$$
\begin{aligned}
H_{(i)+(i+2)} &= H_i + H_{i+2} \\
&= \left(\tfrac{1}{4}U_{i-1} + \tfrac{1}{2}U_i + \tfrac{1}{4}U_{i+1}\right) + \left(\tfrac{1}{4}U_{i+1} + \tfrac{1}{2}U_{i+2} + \tfrac{1}{4}U_{i+3}\right) \\
&= \tfrac{1}{4}U_{i-1} + \tfrac{1}{2}U_i + \tfrac{1}{2}U_{i+1} + \tfrac{1}{2}U_{i+2} + \tfrac{1}{4}U_{i+3}
\end{aligned}
$$

The noise becomes

$$
\begin{aligned}
\sigma^h_{(i)+(i+2)} &= \left[(\tfrac{1}{4}\sigma^u_{i-1})^2 + (\tfrac{1}{2}\sigma^u_i)^2 + (\tfrac{1}{2}\sigma^u_{i+1})^2 + (\tfrac{1}{2}\sigma^u_{i+2})^2 + (\tfrac{1}{4}\sigma^u_{i+3})^2 \right]^{\frac{1}{2}} \\
&= \tfrac{\sqrt{14}}{4}\,\sigma^u = \tfrac{\sqrt{14}}{4}\tfrac{4}{\sqrt{6}}\,\sigma^h \\
&= \sqrt{2\tfrac{1}{3}}\,\sigma^h = 1.53\,\sigma^h
\end{aligned}
$$

– Adding the Hanning tapered channels i and (i+3) gives

$$
\begin{aligned}
H_{(i)+(i+3)} &= H_i + H_{i+3} \\
&= \left(\tfrac{1}{4}U_{i-1} + \tfrac{1}{2}U_i + \tfrac{1}{4}U_{i+1} \right) + \left(\tfrac{1}{4}U_{i+2} + \tfrac{1}{2}U_{i+3} + \tfrac{1}{4}U_{i+4} \right)
\end{aligned}
$$

The noise becomes

$$
\begin{aligned}
\sigma^h_{(i)+(i+3)} &= \left[(\tfrac{1}{4}\sigma^u_{i-1})^2 + (\tfrac{1}{2}\sigma^u_i)^2 + (\tfrac{1}{4}\sigma^u_{i+1})^2 + (\tfrac{1}{4}\sigma^u_{i+2})^2 + (\tfrac{1}{2}\sigma^u_{i+3})^2 + (\tfrac{1}{4}\sigma^u_{i+4})^2 \right]^{\frac{1}{2}} \\
&= \tfrac{\sqrt{12}}{4}\,\sigma^u = \tfrac{\sqrt{12}}{4}\tfrac{4}{\sqrt{6}}\,\sigma^h \\
&= \sqrt{2}\,\sigma^h = 1.41\,\sigma^h
\end{aligned}
$$

So, channelmaps i and (i+3) are independent.

Because the noise is correlated, adding N *adjacent* Hanning tapered channelmaps does not give an increase of the noise with a factor $\sqrt{N}$ but with a factor $\sqrt{N - \tfrac{3}{4} \cdot \tfrac{4}{\sqrt{6}}}$ as is shown below. First the total signal H_N is calculated.

Channel	U_{i-1}	U_i	U_{i+1}	$\cdots$	U_{i+N-2}	U_{i+N-1}	U_{i+N}	
i	$\tfrac{1}{4}$	$\tfrac{1}{2}$	$\tfrac{1}{4}$					
i+1		$\tfrac{1}{4}$	$\tfrac{1}{2}$	$\cdots$				
i+2			$\tfrac{1}{4}$	$\cdots$				
$\cdots$				$\cdots$				
i+N-3				$\cdots$	$\tfrac{1}{4}$			
i+N-2				$\cdots$	$\tfrac{1}{2}$	$\tfrac{1}{4}$		
i+N-1					$\tfrac{1}{4}$	$\tfrac{1}{2}$	$\tfrac{1}{4}$	+
	$\tfrac{1}{4}U_{i-1}$	$\tfrac{3}{4}U_i$	U_{i+1}	$\cdots$	U_{i+N-2}	$\tfrac{3}{4}U_{i+N-1}$	$\tfrac{1}{4}U_{i+N}$	

and thus

$$
H_N = \tfrac{1}{4}U_{i-1} + \tfrac{3}{4}U_i + U_{i+1} + \cdots + U_{i+N-2} + \tfrac{3}{4}U_{i+N-1} + \tfrac{1}{4}U_{i+N}
$$

From this it follows that the noise σ^h_N is given by

$$
\begin{aligned}
\sigma^h_N &= \left[(\tfrac{1}{4})^2 + (\tfrac{3}{4})^2 + (N-2)\cdot 1^2 + (\tfrac{3}{4})^2 + (\tfrac{1}{4})^2 \right]^{\frac{1}{2}} \sigma^u \\
&= \left[N - \tfrac{3}{4} \right]^{\frac{1}{2}} \sigma^u = \left[N - \tfrac{3}{4} \right]^{\frac{1}{2}} \tfrac{4}{\sqrt{6}}\,\sigma^h \\
&= \sqrt{(N - \tfrac{3}{4})B^h}\,\sigma^h
\end{aligned}
$$

However, before the Hanning tapered channelmaps are added to form a total HI map, the continuum must be subtracted and the channelmaps must be cleaned. These operations introduce extra noise in the channelmaps which doesn't behave like a Hanning tapered correlation. In a first approximation the noise added by the cleaning process will be neglected and it will be assumed that a single averaged continuum map will be subtracted from each channelmap (i.e. NPOLY=0 in CONREM). It will be assumed that

the average continuum map is formed by averaging N_1 line free channels at the low velocity end of the datacube and N_2 channels at the high velocity end which gives

$$C_{low} = \tfrac{1}{N_1} \sum_{j=1}^{N_1} H_j \qquad \text{and} \qquad C_{high} = \tfrac{1}{N_2} \sum_{j=1}^{N_2} H_j$$

Since all channels are Hanning tapered the noise in these maps can be calculated according to

$$\sigma_{C_{low}} = \tfrac{1}{N_1} \sqrt{\left(N_1 - \tfrac{3}{4}\right)} \, \sigma^u \qquad \text{and} \qquad \sigma_{C_{high}} = \tfrac{1}{N_2} \sqrt{\left(N_2 - \tfrac{3}{4}\right)} \, \sigma^u$$

The average continuum map to be subtracted is then formed by

$$<C> = \tfrac{1}{2}(C_{low} + C_{high})$$

Since $\sigma_{C_{low}}$ and $\sigma_{C_{high}}$ are independent it follows that the noise $\sigma_{<C>}$ in the finally averaged continuum map is given by

$$\begin{aligned}
\sigma_{<C>} &= \tfrac{1}{2}\sqrt{\sigma^2_{C_{low}} + \sigma^2_{C_{high}}} \\
&= \sqrt{\left(\frac{N_1 - \tfrac{3}{4}}{4N_1^2} + \frac{N_2 - \tfrac{3}{4}}{4N_2^2}\right)} \, \sigma^u \\
&\equiv \mathcal{N}\,\sigma^u
\end{aligned}$$

After subtraction of the continuum the channelmaps only contain signal from the HI emission line. The signal in the channelmaps containing the line emission is now given by

$$\begin{aligned}
L_i &= H_i - <C> \\
&= \tfrac{1}{4}U_{i-1} + \tfrac{1}{2}U_i + \tfrac{1}{4}U_{i+1} - <C>
\end{aligned}$$

Because $\sigma_{<C>}$ is independent from σ_i^u in the velocity range which is not used to form the averaged continuum map, it can be written

$$\begin{aligned}
\sigma_i^l &= \left[\left(\tfrac{1}{4}\sigma^u_{i-1}\right)^2 + \left(\tfrac{1}{2}\sigma^u_i\right)^2 + \left(\tfrac{1}{4}\sigma^u_{i+1}\right)^2 + \sigma^2_{<C>}\right]^{\frac{1}{2}} \\
&= \left[\tfrac{1}{16} + \tfrac{4}{16} + \tfrac{1}{16} + \mathcal{N}^2\right]^{\frac{1}{2}} \sigma^u \\
&= \sqrt{\left(\tfrac{3}{8} + \mathcal{N}^2\right)} \, \sigma^u
\end{aligned}$$

When adding N *adjacent* Hanning tapered and continuum subtracted channelmaps containing the line emission, the signal L_N will be

$$L_N = \tfrac{1}{4}U_{i-1} + \tfrac{3}{4}U_i + U_{i+1} + \cdots + U_{i+N-2} + \tfrac{3}{4}U_{i+N-1} + \tfrac{1}{4}U_{i+N} - N\cdot <C>$$

The noise σ_N^l at each pixel in the final map can be derived analogous to the calculation of σ_N^h and is given by

$$\begin{aligned}
\sigma_N^l &= \left[\left(N - \tfrac{3}{4}\right) + N^2\mathcal{N}^2\right]^{\frac{1}{2}} \sigma^u \\
&= B^h \sqrt{\left(\frac{\left(N - \tfrac{3}{4}\right) + N^2\mathcal{N}^2}{B^h}\right)} \, \sigma^h
\end{aligned}$$

WSRT

PART IV

CHAPTER 3

ERRORS IN MAPS

original article by J.P. Hamaker
with minor changes and updates by O.M. Kolkman.
This is a reproduction of chapter 5b of the old manual. The figures are reproductions[1] of the figures in the old manual. Once the NewStar simulation program N-Simul is available the figures will be remade and parts of this chapter will be rewritten.

3.1 GENERAL REMARK

The purpose of this contribution is to provide a number of illustrations of error patterns generated by a computer or taken from practical examples, which could assist a user in identifying the origin of error patterns he may find in his map. As little theory is given as suffices to understand the pictures and generalize them to so similar but different situations. For more theory, Hamaker (1979) should be consulted, we also refer to chapter 10 'Error recognition' by Ekers in Perley *et al.* (1989).

The effect of errors will be described in terms of error beams, *i.e.* differences $G(l, m)$ between error-corrupted beams and the ideal synthesized beam. Where appropriate, polar beam coordinates (r, ψ) will be used instead of the conventional (l, m). Moreover the projection factor $\sin(\delta)$ is not included, *i.e.* all beams shown either in symbolic or pictorial form are compressed in their North-South dimension.

All computer generated examples shown are for 1×12 hour synthesis with 20 interferometers and telescopes A and B at 72 m and 144 m. The field measures $\frac{0.77°}{\nu}$ by $\frac{0.77°}{\nu} \sin \delta$ (ν is the observing frequency in GHz) and is represented by 256 points in both directions. Toward the edges there may be quantitative differences with the output of a real map making program due to the use of different convolution functions in the visibility plane.

3.2 SYMMETRIES

The basic symmetry properties of the Westerbork error beams are explained in Hamaker (1979). Briefly:
Gain errors produce error pattern symmetric with respect to the beam center, *i.e.*

$$G(l, m) = G(-l, -m)$$

---

[1] The original figures were produced using a specially written simulation program. This program was not available when this documentation was produced so we choose to scan the original images. The horizontal line on the lower half of each figure did already exist on the original images it should be ignored.

Small phase errors result in an anti-symmetrical error beam, *i.e.*

$$G(l, m) = -G(-l, -m)$$

For those phase errors for which the approximation $e^{j\phi} = 1 + i\phi$ is not sufficient, a symmetrical error is superimposed upon the antisymmetric one for small phase errors. For phase errors of about a radian or more the symmetric and antisymmetric contribution become of comparable strength.

In addition, errors that are symmetric or antisymmetric in hour angle (or time with respect to meridian transit) give rise to a similar beam symmetry relative to the horizontal axis, *i.e.*

$$G(l, m) = \pm G(l, -m)$$

3.3   REPRESENTATION OF ERRORS

For each interferometer, gain and phase errors in an interferometer with baseline L may be expanded as a trigonometric series of the hour angle.

$$E_l(h) = a_L + b_L \sin(h) + c_l \cos(h) + ...$$

To an accuracy sufficient for our practical purpose, the second term may be approximately identified with drifts linear in time, the third term with quadratic ones. For geometrical errors (clock, baseline vector, polar axis misalignment, source coordinates), the above formula is exact, see ITR 78 (Brouw, 1974) and ITR 112(Brouw and van Someren Géve, 1973), Brouw's Thesis (1971).

3.4   SINGLE-INTERFEROMETER ERRORS

Although errors are more likely to be associated with a telescope or antenna and hence with a group of interferometers, it is instructive first to consider the single interferometer, which is the basic building block. In the illustration given, the standard Westerbork taper $e^{-ln4\left(\frac{L^2}{L_{MAX}^2}\right)}$ has been applied, with L_{MAX} taken as 1440 m.

3.5   CONSTANT GAIN ERRORS

The contribution from an interferometer with baseline L wavelengths to the synthesized beam is a circularly symmetric beam with a bessel-function cross-section,

$$G_L(r, \psi) \sim J_0(2\pi L r) \tag{3.1}$$

see figure 3.1, a constant gain error produces an error beam of this same form. An extreme case is that of an interferometer completely absent.

3.6   VARYING PHASE ERRORS

Errors Δx (along the baseline) and Δy (in the equatorial plane perpendicular to the baseline) in the assumed baseline vector produce the same effect as errors $\sim \Delta x/L$ in declination, δ, and $\sim \Delta y/L$ in the hour angle, h The resulting error beam is the difference between the shifted beam and the correct one (equation 3.1). For small shifts the error may be approximated by differentiating 3.1 in the direction of the shift, giving

$$G_L(r, \psi) \sim 2\pi L J_1(2\pi L r) \cos(\psi - psi_0) \tag{3.2}$$

where ψ_0 is the position angle of the shift vector. The beam is given in figure 3.1.b.

3.7   CONSTANT PHASE AND VARYING GAIN ERRORS

In spite of its simple form, a phase offset gives rise to the complex pattern of figure 3.2.a. This complexity is due to the u-v discontinuities at $(L, \pm \pi/2)$ where the observed interferometer track and its unobserved hermitian meet. Similar effects occur for gain errors (fig. 3.2.b-d) whenever a linear drift component is present.
Note that a constant phase error $\Delta z \sin(\delta)$ is introduced by an error Δz (in the direction of the celestial pole) in the assumed baseline vector.

3.8   ERRORS IN A FIXED TELESCOPE

All patterns shown oscillate radially at a spatial radian quasi-frequency L, as does the basic J_0 function off equation 3.1. Therefore, the same error occurring in two interferometers with baselines L_1 and L_2 simultaneously gives rise to beats at a quasi-frequency $L_1 - L_2/2$. Figure 3.3.a,b,c show three examples; these should be compared to their single interferometer counterparts, figure 3.1.a and 3.1.b. Note that at a superficial inspection the beat frequency may be thought to be $L_1 - L_2$ rather than half this value.

3.9   ERRORS IN A MOVABLE TELESCOPE

A movable telescope affects 10 interferometers simultaneously, spaced at 144 meter intervals, *i.e.* 2 times the interval for the complete array. Ad a consequence, the beam error is concentrated in rings at intervals of $1/2$ times the standard ring spacing in 12-hour synthesis. In a 'dirty ' map, every other error ring will coincide in position with one of the standard spacing rings and be hidden by it.
examples are shown in figures 3.4a-e. Apart from their radial concentration just discussed, their azimuthal behavior shows similarity to that of the single interferometer counterparts, figures 3.2.a-d.
Rings of this type are commonly referred to as 'AB-rings'.

3.10   SRT BASELINE POLE

The angle between the 'average' baseline of the SRT and the equatorial plane is known as the 'declination of the baseline pole '. It varies slowly in time and must therefore be calibrated for each observation period. Errors in this calibration result in phase errors $E_L \sim L \delta_p \sin(\delta)$. The resulting error pattern consists of an East-West positive/negative tail pair, see figure 3.5.a. Note that the 'dipole' configuration in the center represents a small westward shift. Also note that the pattern is very similar to that of figure 3.4.a, but differs through the absence of an A-B ring (since the error affects all interferometers rather than only one half of them).

3.11   MISSING HOUR ANGLE

It frequently happens that a certain range of hour angles is missing. The resulting beam defect is shown in figure 3.5.b. Its axis has a position angle which differs by 90º from the center of the missing hour angle; its 'opening angle' corresponds to the length of that range.

3.12 $N \times 12$ HOUR SYNTHESIS

All the effects described persist when two or more 12-hour observations are combined in a map, although they are, of course, reduced in size relative to the total synthesized beam.
A more or less new type of error may occur in the form of an imperfect cancellation of the 12-hour grating rings. If the residual rings are not accompanied by other patterns such as AB-rings, they must be due to an error in the calibration in one (or more) of the observations as a whole.

The nature of the error (gain/phase; frequency/clock) can be inferred from the azimuthal variations of the rings by considerations similar to those given above.

3.13   ATMOSPHERE

The most important errors are phase gradients over the array caused by refracting irregularities that vary with time (Hamaker 1978, Hargrave and Shaw, 1978). They provoke radial streaks in the beam; figure 3.5.c shows a practical example where the atmospheric variation occurred mainly on a time scale of 1 to 10 minutes. For longer time scales, the streaks become shorter but more power is built up in them near the beam center (see Hamaker, 1979). Also the grating responses become relatively weaker.

For more information about the effect of the atmosphere see page pagerefAtmospheric corrections of this documentation and e.g. chapter 13 'Propagation Effects' in the book by Thompson *et al.*(1986), chapter 5 'Calibration and Editing' by Fomalont and Perley in the book by Perley *et al.* (1989) and in articles by Spoelstra (1983, 1984 and 1992) which are based on measurements with the WSRT.

3.14   CROSS-TALK

Cross-talk can occur at extreme hour angles (greater than $\approx |75^\circ|$ on a very short baseline (usually 9A=36 meters). When one telescope looks into the back of the other one, ground radiation is *reflected* off the back of one telescope into the aperture of the second one; at the same time, a small fraction of the same radiation leaks through the mesh of the first telescope to give a detectable signal there as well. Thus the two telescopes detect a *correlated* ground radiation signal and consequently the is an *enormous* increase in correlated amplitude. Since this extra signal is detected only at extreme hour angles, it will only appear in maps as a north-south amplitude ripple with a period (in radians) equal to V^{-1} where V (in wavelengths) is the projected interferometer baseline at $h \approx |90^\circ|$ (see figure 3.6)

Note that at hour angles where cross-talk may be detected shadowing (see chapter 9 in part III) will already be so serious that the data is essentially anyway worthless.

3.15   DCB-OFFSETS

DCB-offsets in certain bands can introduce ghost images equivalent to source at certain δ displacement.
In a later version of this documentation we will present more information and a figure.

3.16   DLB-OFFSETS

DLB offsets in sin or cos channel cause ringlike structures. *In a later version of this documentation we will present more information and a figure.*

3.17   TRAVELING IONOSPHERIC DISTURBANCES (TID) AT 92 CM

In a later version of this documentation we will present more information and a figure.

3.18   CLOSURE ERRORS

In a later version of this documentation we will present more information and a figure.

3.19   REFERENCES

Brouw, W.N. (1971): Ph.D. Thesis, University of Leiden.

Brouw, W.N. and van Someren Gréve, H.W.(1973): *NFRA internal tech. report*, **112** (available at NFRA).

Hamaker, J.P. (1979): in *'Image Formation from Coherence Functions in Astronomy'* Ed. Schooneveld, C. D Reidel Publishing Company

Perley, R.A., Schwab, F. and Bridle, A.H. (Editors) (1989): *"Synthesis Imaging in Radio Astronomy"*. Astronomical Society of the Pacific.. ISBN:0-937707-23-6. (see also review in part II Chapter 9.1, Book 2).

Spoelstra, T.A.Th. (1983): *Astron.& Astrophys.* , **120**, pp. 313-321.

Spoelstra, T.A.Th. (1984): Radio Science, **19-no3.**, pp. 779-788.

Spoelstra, T.A.Th. (1992): 'Ionosphere and Troposphere seen through a Radio Interferometer' in *"Remote Sensing of the Propagation Environment"*, AGARD Conference Proceedings 502, Advisory Group for Aerospace Research & Development, Neuilly sur Seine, France.

Thompson, A.R., Moran, J.M. and Swenson Jr., G.W. (1986): *"Interferometry and Synthesis in Radio Astronomy"*. John Wiley & Sons, New York.. ISBN 0-471-80614-5. (see also review in part II Chapter 9.1, book 3).
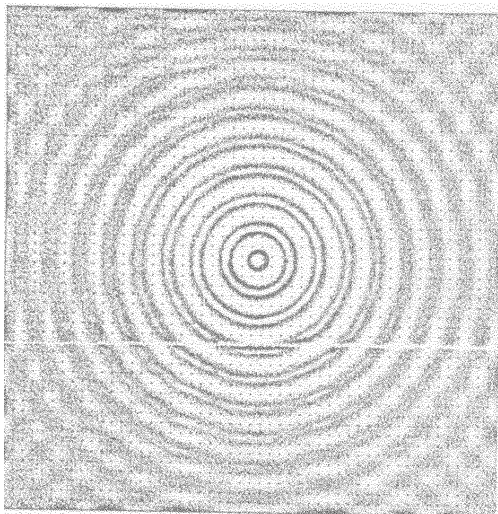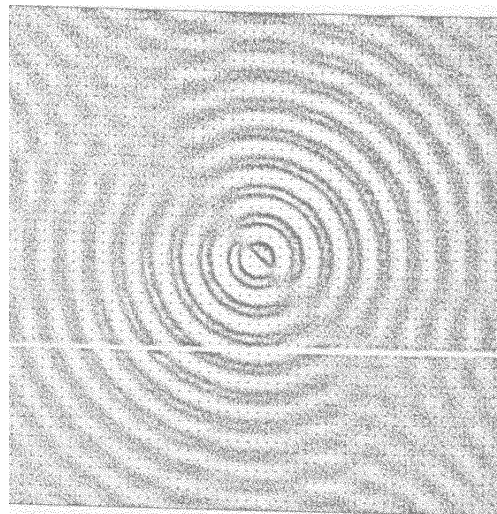
3.1.a   3.1.b

Figure 3.1:
a. The contribution of a single interferometer (360 m spacing) to the WSRT beam. Its cross-section is given by a Bessel function.
b. Contribution from a single interferometer (360 m spacing) for a phase error $1\text{rad} \times (\sin(h) + \cos(h))$
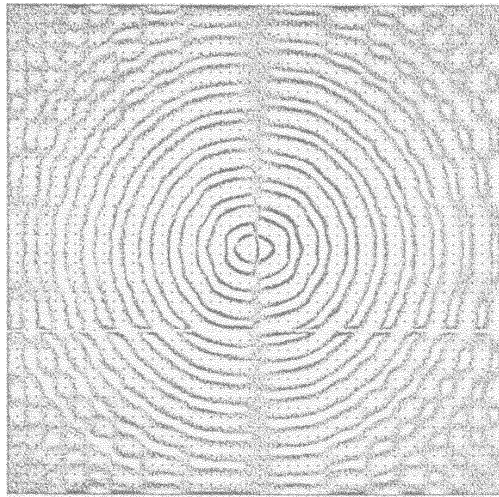
3.2.a
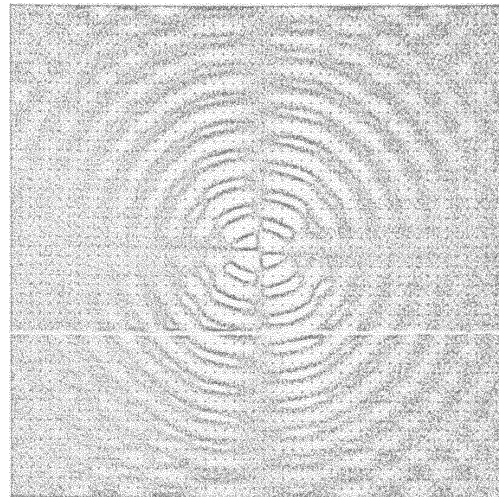
3.2.b
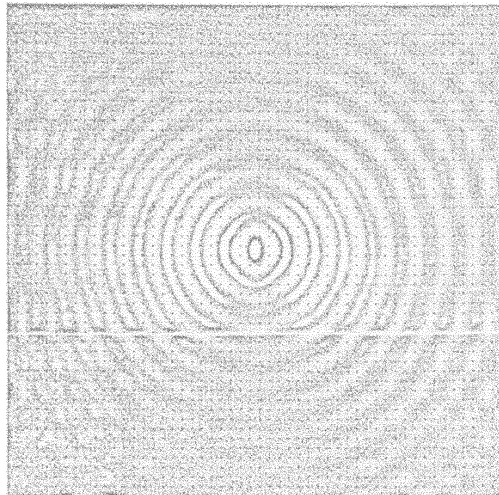
3.2.c
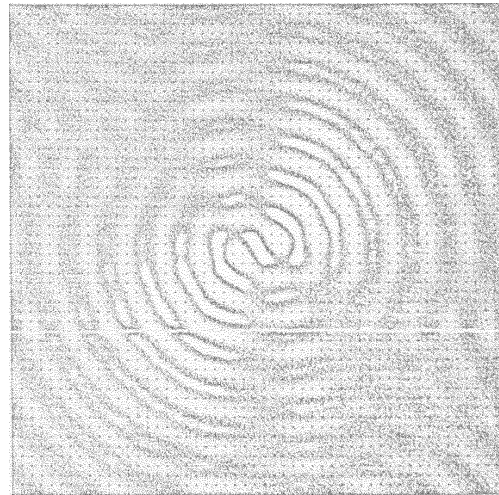
3.2.d

Figure 3.2:
a. The error contribution from a single interferometer (360 m spacing) with a constant phase offset ('collimation error').
b. Error contribution from a single interferometer (360 m spacing) with gain errors varying as $\sin(h)$.
c. Error contribution from a single interferometer (360 m spacing) with gain errors varying as $\cos(h)$.
d. Error contribution from a single interferometer (360 m spacing) with gain errors varying as $\cos(h) - \sin(h) = \cos(h + 45^\circ)$.
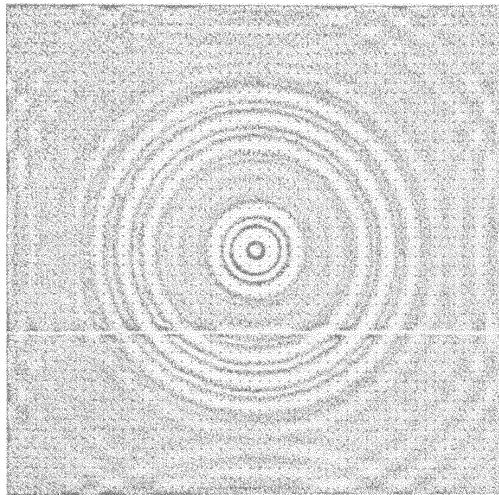
3.3.a
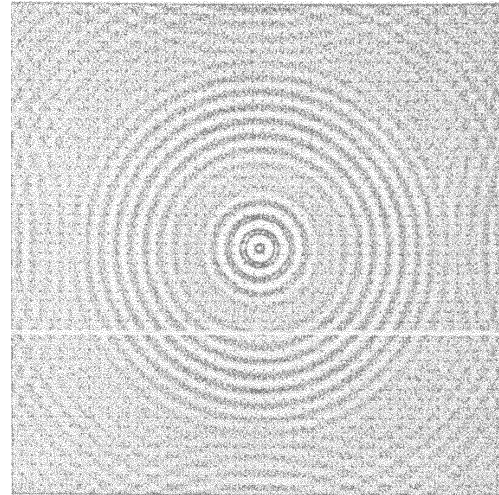
3.3.b
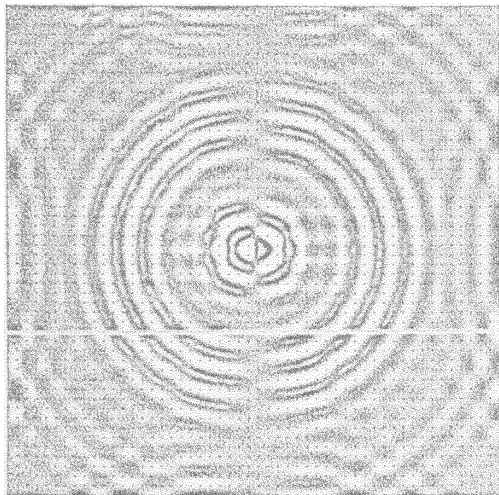
3.3.c

Figure 3.3: Error contribution from a single antenna
(here telescope 7 for examples a and c and telescope 5
for example b)
a. 7A=360 m and 7B=432 m, constant gain offset.
b. 5A=648 m and 5B=720 m, same error.
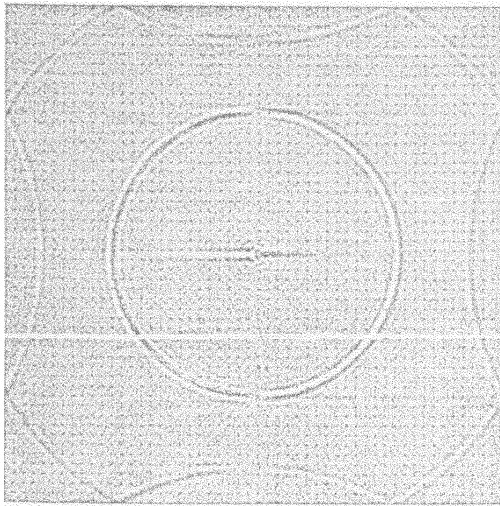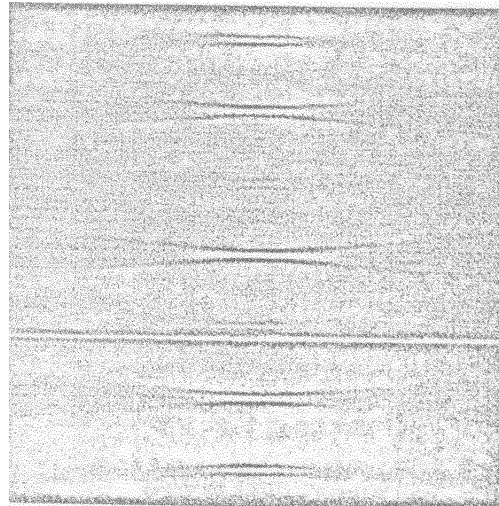**c.**7A=360 m and 7B=432 m, constant phase offset.
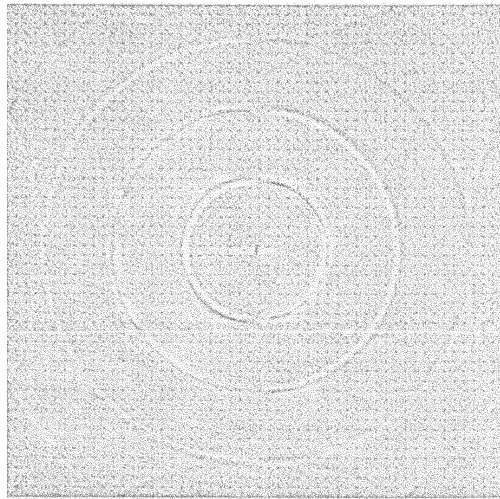
3.4.a
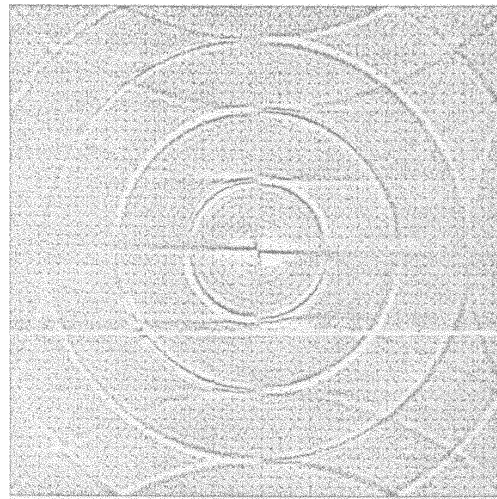
3.4.b
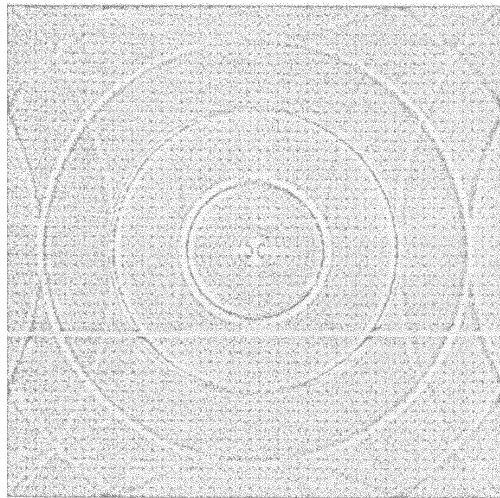
3.4.c
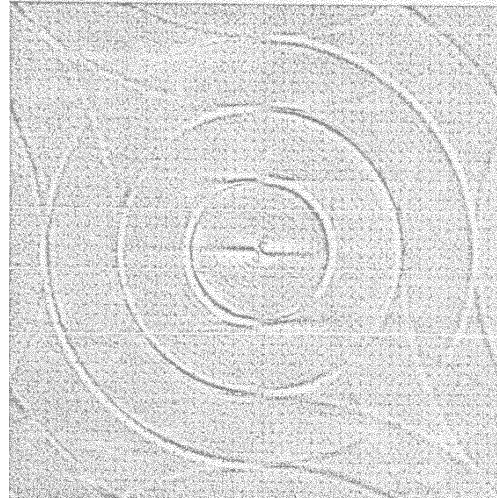
3.4.d
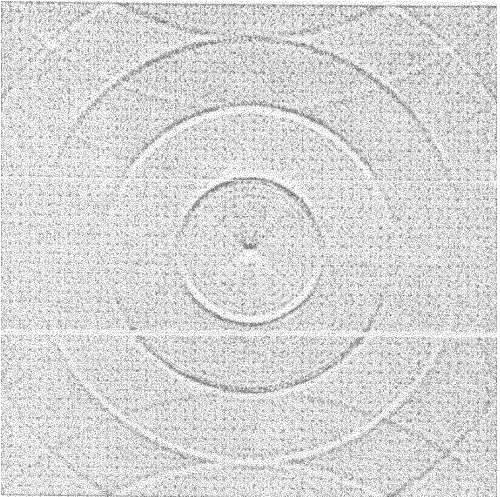
3.4.e

3.4-a. Constant phase offset
3.4-b. Gain error varying as $\sin(h)$
3.4-c. Gain error varying as $\cos(h)$
3.4-d. Gain error varying as $\cos(h) - \sin(h) = \cos(h + 45°$
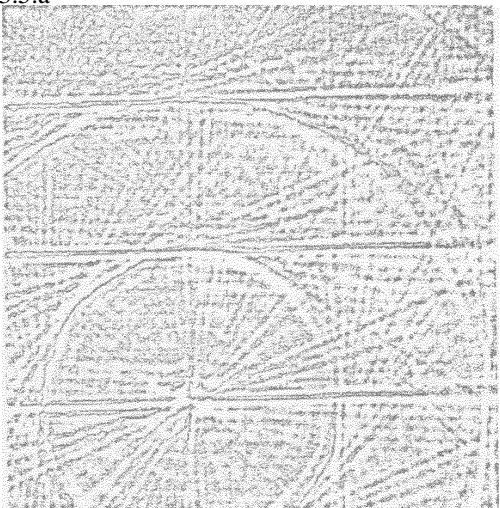**3.4-e.** Phase error varying as $\sin(h)$

Figure 3.4: A-B-rings for various errors in antenna A
at position 72 m

3.5.a

3.5.b

3.5.c

Figure 3.5:
a. Contribution from an error in the declination of the base-line pole, which gives rise to phase offsets in all interferometers proportional to L. The pattern resembles that of a constant phase offset in a movable antenna, but there are no AB rings.
b. The beam defect that results from the absence of hour angles greater than $85°$ in absolute values. The grating responses are much stronger than the normal grating rings.
c. A 21 cm observation of ... (with the point source subtracted) showing the radial streaks characteristics of large-scale atmospheric irregularities. The grating responses of the streaks are much stronger than the normal circular grating rings. The dominant effect in this observation had time scales from 1 to 10 minutes.
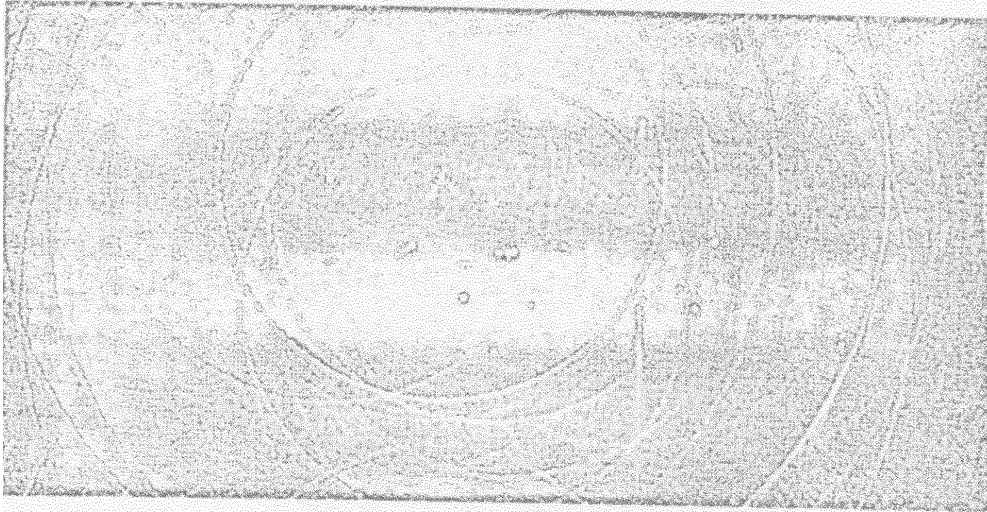
3.6.a
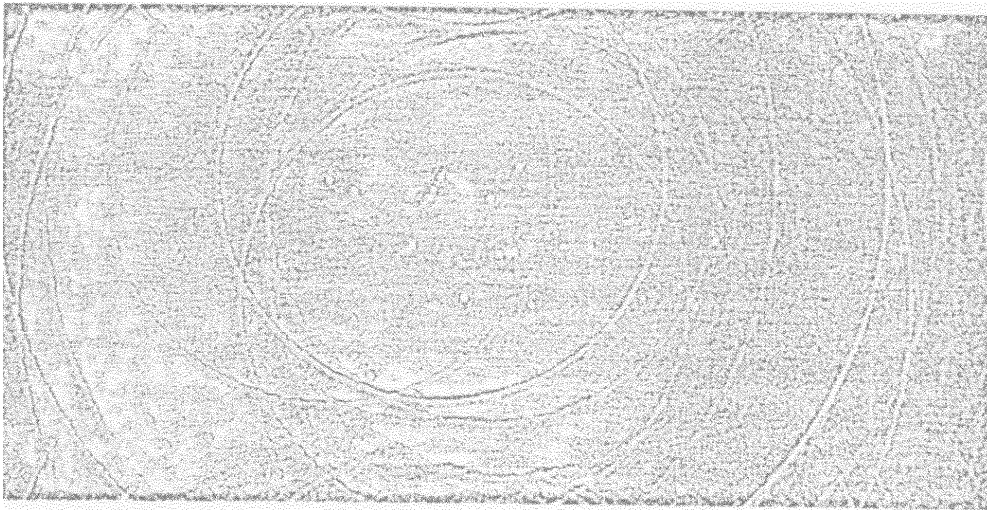
3.6.a

Figure 3.6: A 21 cm observation of the galaxy
NGC3190 at declination 22°
a. the map made from Fourier transforming visibility
data that included cross-talk
b. the same field, but the data affected by cross-talk
were not included in the Fourier transform.